

Research Papers

SOH estimation method for lithium-ion batteries based on an improved equivalent circuit model via electrochemical impedance spectroscopy



Chaofan Li^a, Lin Yang^{a,*}, Qiang Li^a, Qisong Zhang^a, Zhengyi Zhou^a, Yizhen Meng^a, Xiaowei Zhao^b, Lin Wang^b, Shumei Zhang^b, Yang Li^c, Feng Lv^c

^a School of Mechanical Engineering, Shanghai Jiao Tong University, Shanghai 200240, China

^b SAIC Motor Corporation Limited, Shanghai 200030, China

^c Shanghai Qiyuan Green Power Technology Co., Ltd., Shanghai 200001, China

ARTICLE INFO

Keywords:

Electrochemical impedance spectroscopy
Equivalent circuit model
Gaussian process regression
State of health

ABSTRACT

Estimating the state of health (SOH) for lithium-ion batteries (LIBs) has always been one of the most important functions of battery management system (BMS). However, due to the LIBs' complex degradation mechanism, accurate estimation of SOH for the LIBs is still challenging now. As a typical electrochemical system test method, electrochemical impedance spectroscopy (EIS) of LIBs not only contains abundant internal information, but also is not susceptible to external environment. Therefore, in this paper, an EIS based method combining equivalent circuit model (ECM) and data-driven based method is proposed to estimate the SOH of LIBs. Firstly, to improve the fitting performance on EIS, a new equivalent circuit model with an added capacitor (ECMC) was constructed by improving the existing ECMs of LIBs. Then the parameters of the proposed ECMC were identified according to the EIS data, which can reflect the LIBs' degradation better. And the identified parameters, as the inputs to the gaussian process regression (GPR), were used to estimate the SOH of LIBs. The results show that when the parameters identified by the ECMC are used as the inputs of GPR, SOH of LIBs under different temperatures can be accurately estimated. The average root mean square error (RMSE) of this method is only 1.77 %, even for the cell with the worst estimation performance, its RMSE is only 2.95 %.

1. Introduction

Since the dawn of LIBs, they have been widely used in various energy storage devices for the characteristics of relatively high energy density, long cycle life, low self-discharge rate and environment friendliness [1–4]. However, the performance of LIBs will slowly decline with the increase of charge-discharge cycles and some other factors, ultimately affecting LIBs' reliability and security, resulting in potential safety hazards. Therefore, it's of great significance to study the SOH of LIBs for safety and reliability [5].

There are several definitions of LIBs' SOH. And the most commonly used definition is the ratio of current capacity to initial capacity [6], which is described as:

$$SOH = \frac{C_{cur}}{C_{init}} \times 100\% \quad (1)$$

where C_{cur} is the current capacity of LIBs and C_{init} is the initial capacity of

LIBs. Usually, when the current capacity of LIBs drops to 80 % of initial capacity, i.e., $SOH = 0.8$, they are considered to have reached the end of life (EOL), such as LIBs in EVs [7]. However, the criteria for determining EOL of LIBs vary by application [8], $SOH = 0.8$ is just one of the more commonly used standards.

However, accurately estimating LIBs' SOH is not a simple task until now. Firstly, LIBs' degradation is vulnerable to various factors such as temperature, charge and discharge rate, depth of discharge, vibration, side reaction in the batteries and so on. These factors are complexly coupled with each other, making the LIBs' degradation process a highly nonlinear process [9,10], thus it's difficult to build a uniform model to estimate the SOH of LIBs. Secondly, to accurately estimate LIBs' SOH, which kinds of data are used is also important. The mainstream methods now use the external parameters such as current, voltage and temperature during the charge-discharge processes. However, these parameters not only are easily affected by external environment, but also contain insufficient internal information of LIBs, which therefore will affect the final estimation result [11]. The application of EIS in LIBs helps solve

* Corresponding author.

E-mail address: yanglin@sjtu.edu.cn (L. Yang).

these problems. As a non-invasive method [12], EIS includes sufficient internal information about the LIBs than time domain data [13]. At the same time, it's not easily affected by the external environment, with better stability and reliability.

As a classical test method, EIS has been widely used to study electrochemical system for a long time. The EIS of LIBs can be obtained by applying a small sinusoidal current excitation and then measuring the response voltage [14]. Its principle can be described as:

$$Z_{\text{Bat}} = \frac{U_{\text{res}}}{I_{\text{exc}}} = \frac{U_0 e^{j(wt+\varphi)}}{I_0 e^{jwt}} = Z_0 e^{j\varphi} = Z_0 (\cos\varphi + j\sin\varphi) \quad (2)$$

where Z_{Bat} is the impedance of LIBs calculated by the excitation current I_{exc} and the response voltage U_{res} . And w is the angular frequency of the excitation current, Z_0 is the modulus of Z_{Bat} . It can be seen that compared to response voltage, the excitation current has a phase lag φ , which makes the impedance of LIBs finally appear as a complex number.

As LIB degrades, a series of changes will occur within it, which will be reflected in its EIS data. By analyzing the EIS dataset in Ref [15], the variation trend of LIBs' EIS data with the number of charge-discharge cycles can be obtained. Fig. 1 was drawn by using the EIS data of a battery in this dataset after being fully charged under different charge-discharge cycles. As can be seen from Fig. 1, with the number of charge-discharge cycles of LIB increasing, its EIS data changes significantly. In the ultra-high frequency region, the curve shifts to the right as the LIB degrades, meaning the internal resistance of LIB increases. In the high and middle frequency regions, the two semicircles representing the solid electrolyte interphase (SEI) film inside LIB and the charge transfer process between the electrolyte and electrode also change, especially the latter's radius increases obviously with the degradation of battery. And changes also occur in the low frequency region, the curve tends to move to the upper right with LIB degrading, both the real and imaginary part of the LIBs' impedance are increased, which means that the diffusion process of Li-ions in the electrolyte is also affected, the overall trend is increasingly difficult to diffuse. Therefore, through introducing the EIS, it is expected that the LIBs' SOH estimation accuracy can be improved.

1.1. Literature review

There have been numerous studies on using EIS data to estimate the LIBs' SOH until now. According to the methods used, they can be divided into three categories: physics-based model methods, ECM based methods and data-driven based methods [16].

EIS can reflect the reaction processes inside the LIBs well, so it is often used to construct the physical-based models such as Thevenin

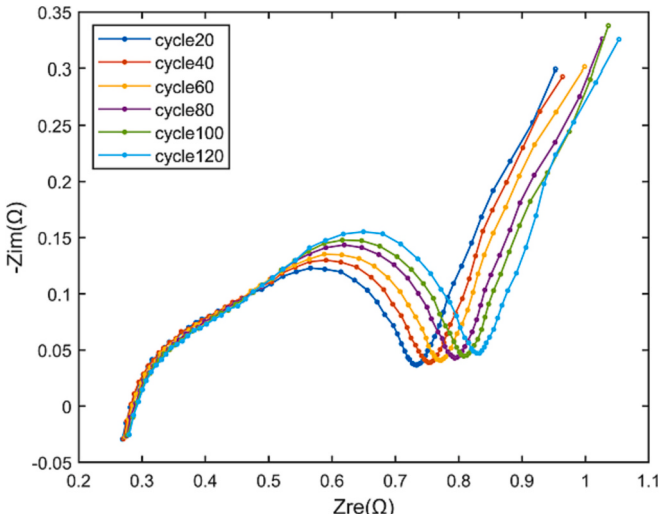


Fig. 1. Impact of SOH change on EIS.

model, run-time based electrical model and combined electrical model [17]. For instance, Landinger et al. [18] took the LIBs' geometry, temperature and state of charge (SOC) into consideration and constructed a physical-based high frequency battery model named HF EEC model based on the EIS data for cylindrical LIBs in the frequency range of 1KHz-300 MHz, which can be used for simulating highly dynamic battery applications. Duan et al. [19] demonstrated the parameter identification process by coupling the proposed physics-based model with EIS data for an NMC523/Li half-cell tested under different Li-ion stoichiometry and proved the effectiveness and accuracy of this model by comparing it with the traditional one. However, although physical-based models can deeply reveal the reaction mechanisms and structure changes inside LIBs, it's too difficult for any physical-based models to fully accommodate them, due to the LIBs' complex internal structure and various reactions coupling with each other.

The ECM based methods are also used to estimate the SOH of LIBs due to the low computational complexity and reasonable accuracy [20]. A typical ECM usually consists of inductor, resistor, capacitor, constant phase element (CPE) and Warburg element [21]. And EIS data is often used to calculate the parameters of the above components in the ECM. For example, Galeotti et al. [22] obtained the parameters of the ECM by fitting EIS data, then the LIBs' diagnostic map for SOH under different SOC and ohmic resistance was constructed. As long as the SOC and ohmic resistance of the LIBs were known, the current number of charge-discharge cycles can be obtained by querying the diagnostic map. Li et al. [23] found out the ECM with the best fitting performance for EIS by comparing the fitting errors of the commonly used ECMS, and constructed the exponential relationship between the LIBs' internal resistance and SOH at different temperatures. The methods based on the ECM are simple to operate and can obtain the variation trend of LIBs' internal characteristics such as electrolyte resistance during the aging process. But their problems cannot be ignored either. One of the most prominent problems is that different kinds of LIBs have different internal reaction mechanisms, making it difficult to apply the mathematical relationship between the SOH and ECM parameters proposed from one type of LIB to another. This limits the applicability of ECM based methods and is an urgent problem to be solved.

For the model-free characteristic [24], high flexibility [25] and powerful nonlinear behavior capture ability [26], data-driven based methods are also frequently used to estimate LIBs' SOH. These methods can be divided into three categories based on the type of input data. The first kind of method is to estimate the SOH of LIBs by taking the impedance at all measured frequencies in the selected spectrum as inputs to the model. Zhang et al. [15] measured the EIS data of 12 batteries in the frequency region from 0.02 Hz to 20KHz under different temperatures and SOH. Then all the real and imaginary parts of EIS data were selected as inputs to the GPR to estimate the LIBs' SOH. Obregon et al. [27] also used the whole frequency region EIS data as the inputs of a convolutional autoencoder to extract the features automatically, then these features were used in a deep neural network to estimate the SOH. The second kind of method is selecting specific EIS spectral characteristics as inputs. In this class of methods, the selected spectral characteristics are also different. For instance, Jiang et al. [28] found that the middle and low frequency regions of EIS changed significantly with the degradation of LIBs, so the impedance at 1 Hz, 5 Hz and 10 Hz were selected as inputs of the SOH estimation model. And Chang et al. [29] believed that the impedance data corresponding to 0.2 Hz, 2.16 Hz, 17.8 Hz and 20KHz had the strongest relationship with the LIBs' degradation, so they were selected as the inputs of Elman neural network to estimate the SOH. And the third kind of method is different from the above two methods in selecting the inputs of data-driven model. Some health indicators (HIs) are extracted from EIS data instead of using it directly, then the HIs are used to estimate the LIBs' SOH. For example, Zhou et al. [30] analyzed the geometric shape of EIS's Nyquist plot minutely. Then they used semicircles to fit the Nyquist curve of middle and high frequency regions, chose the two semicircles'

center and radius as HIs to estimate the SOH via Recurrent-GPR. Su et al. [31] calculated six HIs related to LIBs' SOH based on the EIS data in low frequency region, such as curve slope, etc., and combined them with EIS data in low frequency region to estimate SOH. In a word, the data-driven based methods can well reflect the nonlinear relationship between EIS and SOH of LIBs. However, due to the problems such as high requirements on data quality and quantity [32,33], unexplained internal process [34] and high requirements on the input features [35], the data-driven based methods are still very rare in practical applications.

1.2. Contributions in this work

In order to solve the problems mentioned in the above methods, the ECMC-GPR method is proposed in this paper. This method combines the ECM based method and data-driven based method together. Firstly, an improved ECM model, ECMC, was proposed, and it was used to extract the features from LIBs' EIS data. Then these features were used as inputs into GPR to estimate the SOH of LIBs. The effectiveness of the proposed method was verified by experiments at last. The main contributions of this paper can be summarized as follows:

1. Based on the inference that an electrical double layer (EDL) effect like SEI film exists in the LIBs when they are excited by the external low frequency signal, an improved ECM named ECMC was constructed. The verification results show that compared with the existing ECMs, the improved ECMC can greatly improve the fitting performance of the EIS data and better reflect the internal structure and reaction processes of LIBs.
2. The improved ECMC based method and the data-driven based method were combined together for the LIBs' SOH estimation via EIS. In this way, the ECM based methods' shortcoming of poor generalization and the data-driven based methods' shortcoming of requirement of high-quality input features can be overcome at the same time, making the estimation results of LIBs' SOH more convincing.
3. The parameters of the proposed ECMC were identified using EIS data, and the SOH of LIBs was estimated successfully by using these parameters as the input features of GPR. The average RMSE of this method is only 1.77 %, which proves the feasibility of the proposed ECMC-GPR method.

1.3. Organization of this paper

The remainder of this paper is organized as follows. In Section 2, the methods used in this paper are presented, including the introduction of dataset and data preprocessing, constructing ECMC and the SOH estimation method GPR. And Section 3 gives the variation trend of ECMC' parameters with battery degradation and the SOH estimation results. At last, conclusion is summarized in Section 4.

2. Methodology

2.1. Dataset and data preprocessing

Dataset used in this paper, which comes from Ref [15], contains EIS data from 12 45mAh Eunicell LR2032 Li-ion coin cells at three different temperatures (25, 35, 45 °C) named 25C01-08, 35C01-02 and 45C01-02. The cell chemistry is LiCoO₂/graphite. The EIS data of LIBs in the spectrum range of 0.02 Hz-20KHz were measured 9 times in different states during one charge-discharge process, respectively named state1-9, and the excitation current used was 5 mA. Among them, state1 was measured before LIBs were charged, state5 was measured after LIBs were fully charged and left for 15 min, state 9 was measured after the LIBs were fully discharged and left for 15 min, and the remaining six states were measured during the charge-discharge process.

In order to observe the differences between different states' EIS data,

the 25C04 battery's EIS data under 9 states in the first charge-discharge cycle were selected to draw the Nyquist plot. As shown in Fig. 2, EIS data measured during charge-discharge process (state2-4,6-8) are unstable and differ greatly from the typical EIS Nyquist plot. That's because of the polarization effect of LIBs during charge-discharge process. Due to the small excitation current used to measure the EIS, the response voltage is small either, which is easily drowned in the noise caused by polarization effect. In addition, Fig. 2 also shows that the deformation of EIS is mainly concentrated in the middle and low frequency regions (below 20 Hz), so it can be inferred that the polarization effect mainly affects the Li-ions' diffusion process in the electrolyte and the charge transfer process occurs in the interface between electrode and electrolyte. Therefore, state1,5,9 are better choices compared with other states to estimate LIBs' SOH. Considering that it's difficult to reach 0 % SOC for actual vehicles, so the state5, which is the EIS data measured when the SOC is 100 % was chosen to estimate the SOH. This means that the EIS data of the LIBs can be measured after they are fully charged and left for 15 min, then these data can be used to estimate the SOH. This is very consistent with the actual situation and conductive to the application and promotion of EIS in reality.

Charge and discharge amount of these batteries after each charge-discharge cycle are also provided in this dataset. Considering the capacity regeneration phenomenon [36] and the definition of battery's capacity, the discharge amount of these batteries in each charge-discharge cycle was chosen as the capacity data. In addition, although the LIB reaches its EOL when the actual capacity drops to 80 % of its initial capacity, the proportion of data that do not reach EOL in the dataset is not large actually, so the data whose capacity higher than 25mAh were chosen to be used ultimately in this paper, they account for a large proportion of the total data.

When the ECM is used to fit the EIS data, an inductor is usually connected in series in the model to represent the inductance characteristic of the batteries' collector and the external conductor. However, it is generally believed that the batteries' collector and external conductor do not change during the process of degradation. Therefore, the inductance characteristic hidden in EIS data can be eliminated by data preprocessing to reduce the complexity of ECM. The impedance expressions of battery and inductor are defined as:

$$Z_{\text{Bat}} = Z_{\text{re}} + jZ_{\text{im}} \quad (3)$$

$$Z_L = j2\pi fL \quad (4)$$

where Z_{Bat} is the impedance of battery, it's composed of the real part of impedance Z_{re} and imaginary part of impedance Z_{im} . Z_L is the impedance of inductor and f is the frequency of excitation signal, L is the inductance of external conductor and collector. From Eq. (4), it can be found that the existence of inductor affects the imaginary part of battery's impedance. Therefore, in order to eliminate the influence of inductor on the fitting performance, the impedance data of battery should be pre-processed as follows:

$$Z_{\text{Bat}} = Z_{\text{re}} + j(Z_{\text{im}} - 2\pi fL) \quad (5)$$

After preprocessing the EIS data, inductor can be removed from the model when constructing ECM.

2.2. Construct ECM based on EIS

How to construct an ECM that can accurately fit the EIS data of all LIBs is still a problem at present. Scholars now often construct the corresponding ECM by studying the internal structure and reaction processes of LIBs. For example, the charge transfer process and the SEI film inside LIBs can often be simulated with a resister and a capacitor or CPE connected in parallel, and the diffusion process of Li-ions in the electrolyte can be simulated using Warburg element [30]. Correspondingly, the physical and chemical reactions and changes in the LIBs can also be

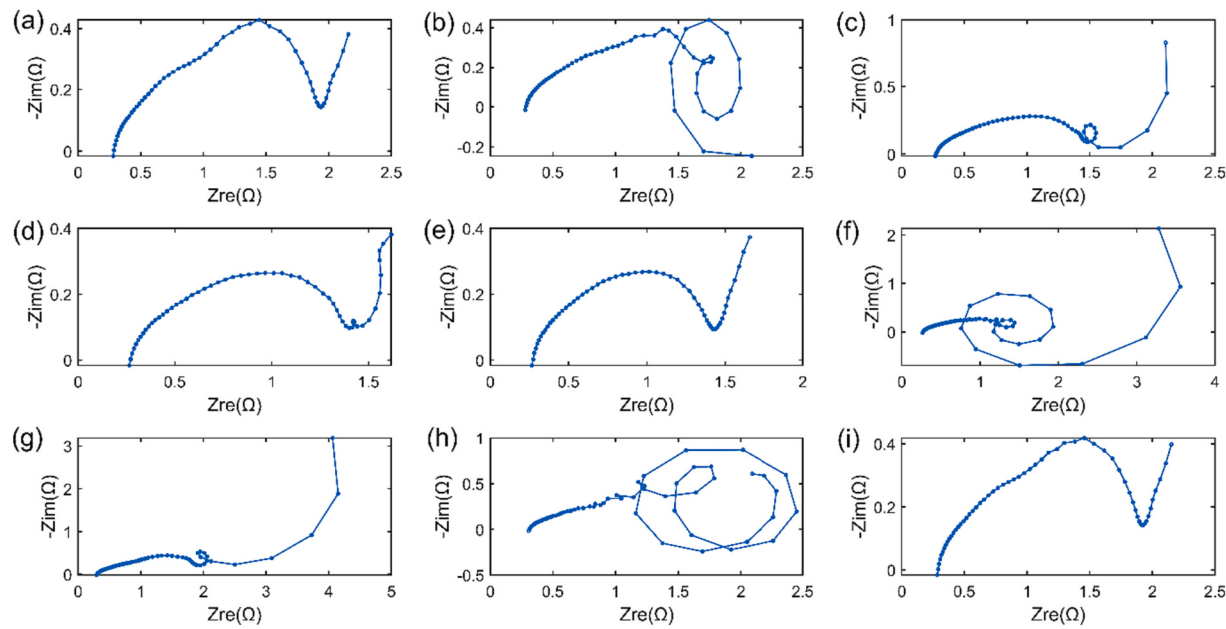


Fig. 2. Nyquist plot of EIS data for 25C04 battery's first charge-discharge cycle measured at different states: (a)-(i) state1–9.

reflected by the parameters' change of the ECM. During the degradation of LIBs, a series of changes will occur, such as the increase of SEI film's thickness and internal resistance [37], which will change the corresponding components' parameters of the ECM, making it feasible to estimate the LIBs' SOH by using the parameters of ECM.

Therefore, the primary problem of using ECM's parameters to estimate LIBs' SOH is constructing an ECM which can fully reflect LIBs' internal structure and reaction processes. Since the internal structure and reaction processes of LIBs are included in their EIS data, it's also required that the frequency response curve of the constructed ECM can fit the EIS well, this is our goal to construct an ECM based on EIS data. Fig. 3 shows some commonly used ECMs. In general, these ECMs can be roughly divided into four parts according to the series order, which are the modeling description of the LIBs' ohmic resistance, SEI film, charge transfer process and the diffusion process of Li-ions in the electrolyte. However, the components and connection methods used in these models are different. Among these ECMs, model (a)-(d) are connected in the same way. Compared with model (a), models (b) and (c) replace all or part of the capacitors with CPEs, mainly because CPE can better describe

the dispersion effect of the solid electrode, but it also leads to an increase in computational complexity. The main change in model (d) is the replacement of the Warburg element with a capacitor, aiming to simplify the model and calculation. Compared with model (a)-(d), model (e) and (f) show a big difference in connection method, which is because the charge transfer process and Li-ions diffusion process in LIBs are considered to be a mutually coupled process when two models are constructed. To verify the fitting performance of these models, about 50 EIS data were randomly selected from the dataset to fit these models by using the EIS data analysis software ZSimpWin. The fitting errors are shown in Table 1. The indexes used are defined as:

Table 1
Fitting error on EIS data for the commonly used ECMs.

Model	(a)	(b)	(c)	(d)	(e)	(f)
RMSE _{re}	0.0263	0.0099	0.0166	0.0189	0.0141	0.0243
RMSE _{im}	0.0256	0.0117	0.0211	0.0123	0.0161	0.0241

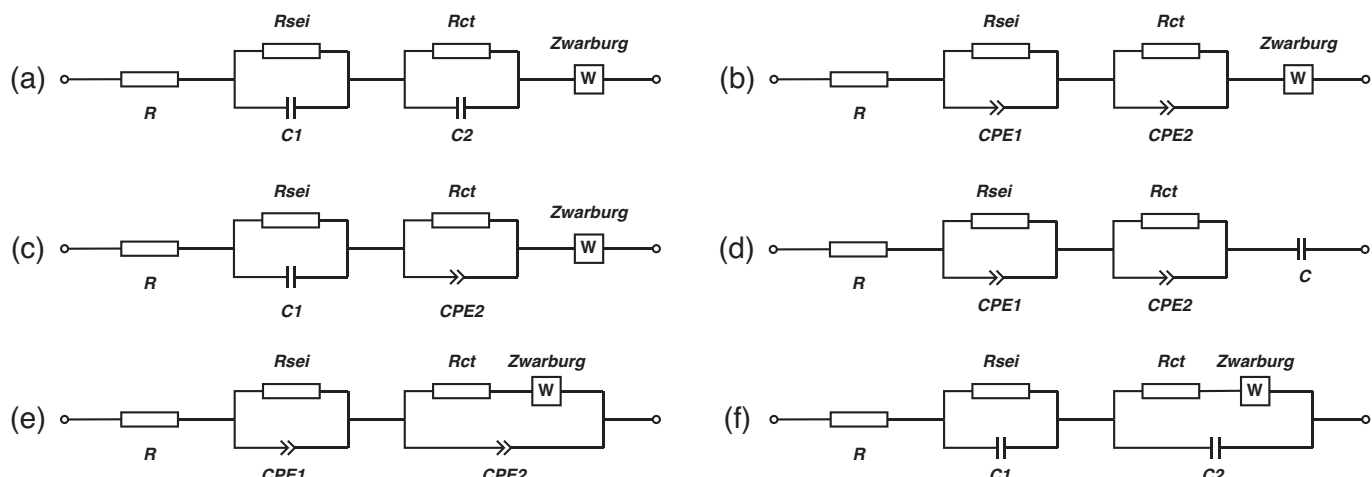


Fig. 3. Some commonly used ECMs. (a)-(d) R : ohmic internal resistance, R_{sei} connects with C_1 or CPE_1 in parallel; SEI film, R_{ct} connects with C_2 or CPE_2 in parallel; charge transfer process, $Z_{Warburg}$ or C : diffusion process of Li-ions in the electrolyte. (e)-(f) R : ohmic internal resistance, R_{sei} connects with C_1 or CPE_1 in parallel; SEI film, R_{ct} connects with $Z_{Warburg}$ in series then connects with C_2 or CPE_2 in parallel; coupled charge transfer process diffusion process of Li-ions in the electrolyte.

$$RMSE_{re} = \sqrt{\frac{\sum_{i=1}^N (Z_{re_measure}(i) - Z_{re_fit}(i))^2}{N}} \quad (6)$$

$$RMSE_{im} = \sqrt{\frac{\sum_{i=1}^N (Z_{im_measure}(i) - Z_{im_fit}(i))^2}{N}} \quad (7)$$

where $Z_{re_measure}$, $Z_{im_measure}$ are the real and imaginary parts of measured EIS data and Z_{re_fit} , Z_{im_fit} are the real and imaginary parts of fitted EIS data using ECMs. By using these measured data and fitted data, the fitting error of real parts of EIS data $RMSE_{re}$ and imaginary parts of EIS data $RMSE_{im}$ can be obtained.

It can be seen from Table 1 that the fitting error of model (b) is minimal, which is marked in bold. In order to observe this ECM's fitting performance intuitively, we selected it to fit the EIS data of the 25C01 battery's first charge-discharge cycle and the other three CR2016 Li-ion coin cells named battery1–3. These three cells' chemistry is MnO_2/Li , which is different from the battery used in dataset. And battery1–3 were tested after different charge-discharge cycles by ModuLab XM electrochemical test system in our Lab. The frequency region of external excitation for the other three batteries also was 0.02 Hz-20KHz. The fitting results are shown in Fig. 4, where the blue line represents actual EIS data and the red one represents fitting result. It can be seen from Fig. 4 that even if ECM with the smallest fitting error is selected, fitting result is still unsatisfactory, and its error is mainly concentrated in the low frequency region, so it's necessary to continue to improve the ECM in this aspect.

The fitting error of ECM (b) (i.e., the model (b) in Fig. 3) is mainly concentrated in the low frequency region, which is generally thought to represent the diffusion process of Li-ions in electrolyte. And Warburg element is used to simulate it in ECM (b), its impedance $Z_{warburg}$ is defined as:

$$Z_{warburg} = \frac{\sigma}{\sqrt{w}}(1-j) \quad (8)$$

where σ is Warburg coefficient and w is the angular frequency of excitation signal. According to Eq. (8), the spectrum response of LIBs in low

frequency region should be a 45° straight line on the Nyquist plot. But it's obvious that the actual measured curves of these batteries in Fig. 4 all deviate from 45° , resulting in poor fitting performance of the ECM (b). This means that there are other factors affect the EIS of LIBs besides the diffusion effect of Li-ions in the electrolyte under low frequency excitation.

To explain this deviation phenomenon, we try to make an inference based on the internal reactions of LIBs when they are excited by low frequency signal. Here, Fig. 5(a) is used to describe these internal reaction processes. The small black circles at negative electrode represent C atoms, they are arranged regularly to form graphite. And the large white circles represent Li, they are embedded in the pore of graphite. While the large black circles in the electrolyte represent the Li-ions. Different from the reactions under the high frequency external excitation only need to consume Li-ions near the electrodes, when the low frequency excitation is applied, as shown in Fig. 5(b), due to the long duration T of one excitation cycle, battery seems like to be in the state of charging and discharging, we call these state exc-charge and exc-discharge state. Assuming that battery in Fig. 5(a) is under the exc-discharge state, the amount of Li-ions near the positive electrode is not enough to support the long-term electrode reactions, so there must be additional sources of Li-ions to support these reactions. One of the sources is Li embedded in the graphite, they will lose electrons to form Li-ions. Then the electrons travel along the external wire toward positive electrode while the Li-ions diffuse in the electrolyte toward the positive electrode due to the difference in concentration. However, the electrons' moving speed V_2 is much higher than Li-ions' diffusion speed V_1 in the electrolyte. So some Li-ions will gather in the negative electrode while some electrons that do not participate in the reactions will gather in the positive electrode, just like the two ellipses circled by red dotted line in Fig. 5(a). This phenomenon is very similar to the accumulation of charge on both sides of SEI film in LIBs under high frequency excitation, which is called EDL [38]. In ECM, in order to simulate this EDL effect of SEI film, a capacitor or CPE is usually connected to resistor in parallel. Therefore, here we also consider connecting a capacitor to Warburg element in parallel to simulate the similar phenomenon of LIBs under

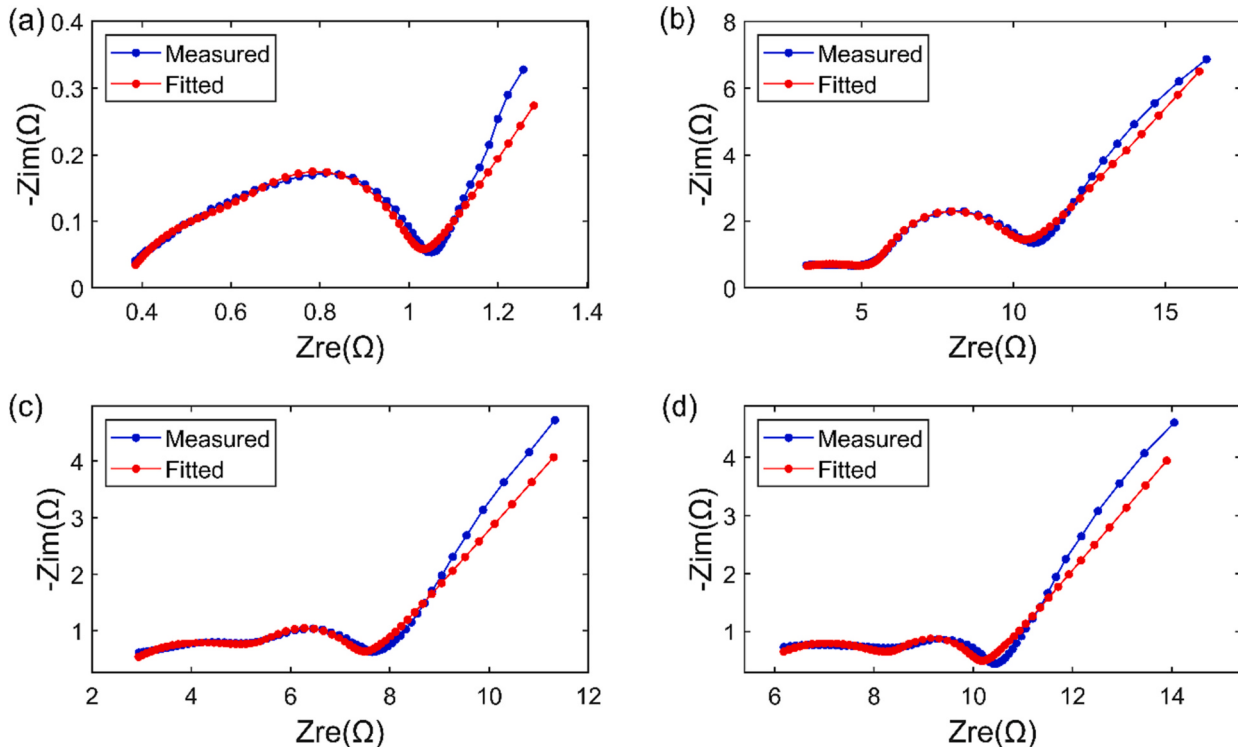


Fig. 4. (a) Fitting result of ECM (b) on the EIS data of 25C01 battery's first charge-discharge cycle. (b)-(d) Fitting results of ECM (b) on the EIS data of battery1–3.

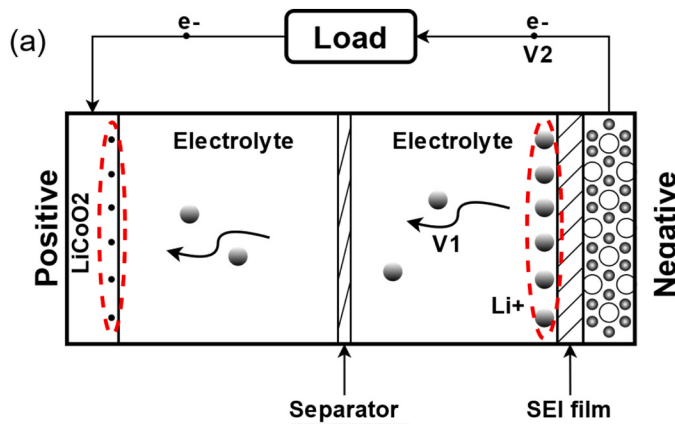


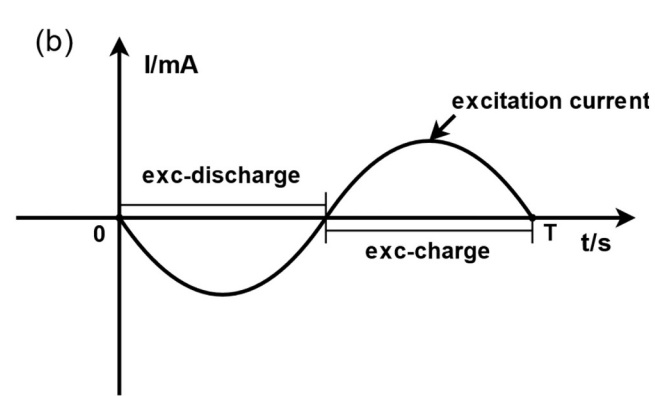
Fig. 5. (a) Internal reaction processes of LIBs excited by low frequency signal (b) state of battery during one excitation cycle.

low frequency excitation based on ECM (b). Fig. 6 is the ECM with an added capacitor named ECMC that we finally constructed. Since the impedance expression of CPE is far more complex than that of a pure capacitor, it will not only increase the difficulty of using ECM to fit EIS data, but also reduce the robustness of fitting. Therefore, one of the CPEs was replaced with a pure capacitor in this ECMC.

In order to verify the performance of the ECMC, and for fair comparison, it was also used to fit these randomly selected EIS data from the dataset and the battery1–3’ EIS data. The fitting errors of ECM (b) and ECMC are shown in Table 2. And when a model has a smaller error for the same battery, its error will be marked in bold in the table. Obviously, compared with ECM (b), this newly proposed ECMC can greatly reduce the fitting error on EIS data for all the batteries. Among them, the fitting error decreases the most for these randomly selected batteries’ EIS data in the dataset, which can reduce to 20 % of the primary error. Even for the battery3, whose fitting error decreases the least, can still reduce to half of the primary error. In addition, the 25C01 battery’s first charge-discharge cycle’s EIS data and battery1–3’ EIS data were also selected to present the fitting performance of proposed ECMC, as shown in Fig. 7. Where the blue line is actual EIS measurement result and the red line is fitting result. Compared with Fig. 4, it can be seen that ECMC can greatly improve the problem of deviation in low frequency region. And fitting performance in full frequency region is also improved. The chemistry between 25C01 battery and battery1–3 is different, which indicates that the ECMC model can accurately fit different types of LIBs and has a certain generalization ability.

2.3. Gaussian process regression

Compared with machine learning algorithms such as neural network, the GPR method has the advantages of easy implementation, flexible non-parametric inference ability, and adaptive acquisition of hyperparameters. And the predicted result can make a probabilistic interpretation of the expected output [31]. Gaussian process is used in GPR to implement non-parametric regression. The key idea of it is to assume that the function $f(x)$ to be solved satisfies the GP probability distribution as shown in Eq. (9) rather than postulating a parametric form for the function $f(x, \phi)$ and estimating the parameters ϕ [39].



$$f(x) \sim GP(m(x), \kappa(x, x'))$$

$$m(x) = E[f(x)]$$

$$\kappa(x, x') = E[(f(x) - m(x))(f(x') - m(x'))^T] \quad (9)$$

where x and x' are the known observed variables and unknown variables that input to GPR, respectively. $m(x)$ and $\kappa(x, x')$ represent the mean and covariance function respectively.

The first task to use GPR is making a prior estimate of $m(x)$ and $\kappa(x, x')$, since GPR is a non-parametric model, it is always possible to traverse the entire parameter space, so here we can set the mean function $m(x)=0$ to simplify the calculation. Then a posterior adjustment to the hyperparameters in $m(x)$ and $\kappa(x, x')$ according to the observed values after obtaining the observations is needed. This is the general process of training GPR. After training, using GPR to make predictions works as follows. Suppose we have a set of observations $\{(x_i, y_i), i = 1, 2, 3, \dots, n\}$ and the relation between them is $y_i = f(x_i + \epsilon_i)$, where $\epsilon_i \sim \mathcal{N}(0, \sigma^2)$ is an independent and identically distributed Gaussian noise. The outputs $Y = [f(x_1), f(x_2), \dots, f(x_n)]$ are modelled as a Gaussian random field $f \sim \mathcal{N}(0, K)$, where $K_{ij} = \kappa(x_i, x_j)$ and is the covariance function mentioned earlier, also known as the kernel function. The covariance between x_i and x_j calculated by the kernel function is a measure of how close the two points are. Since the observation set $\{(x_i, y_i), i = 1, 2, 3, \dots, n\}$ and the data needed to estimate (x^*, y^*) both conform to the GP distribution, their joint distribution also conforms to the GP distribution shown in Eq. (10).

$$\begin{bmatrix} Y \\ y^* \end{bmatrix} \sim \mathcal{N}\left(0, \begin{bmatrix} K(X, X) + \sigma^2 I & K(X, x^*) \\ K(x^*, X) & K(x^*, x^*) \end{bmatrix}\right) \quad (10)$$

where I is the identity matrix. So the predicted mean \bar{y}^* for the x^* is:

$$\bar{y}^* = K(x^*, X)(K(X, X) + \sigma^2 I)^{-1} Y \quad (11)$$

and the predicted variance Δ^2 is:

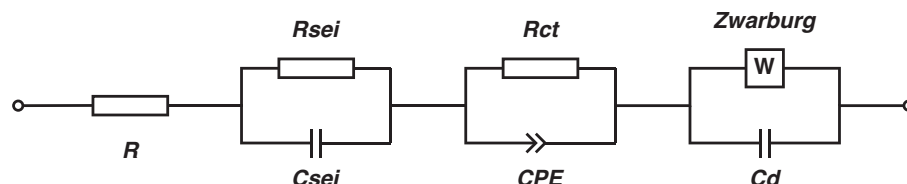
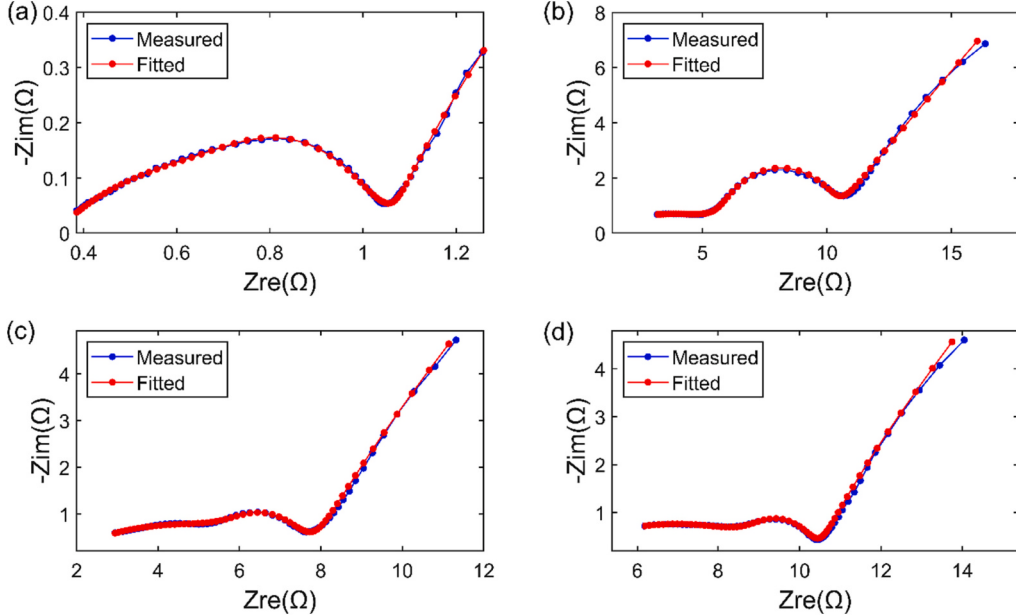


Fig. 6. ECMC constructed in this paper.

Table 2

Comparison of fitting error between ECM (b) and proposed ECMC.

Model	ECM(b)				Proposed ECMC			
Battery	batteries in dataset	battery1	battery2	battery3	batteries in dataset	battery1	battery2	battery3
RMSE_re	0.0099	0.0830	0.1020	0.1044	0.0028	0.0343	0.0486	0.0642
RMSE_im	0.0177	0.1407	0.1610	0.1172	0.0026	0.0374	0.0437	0.0370

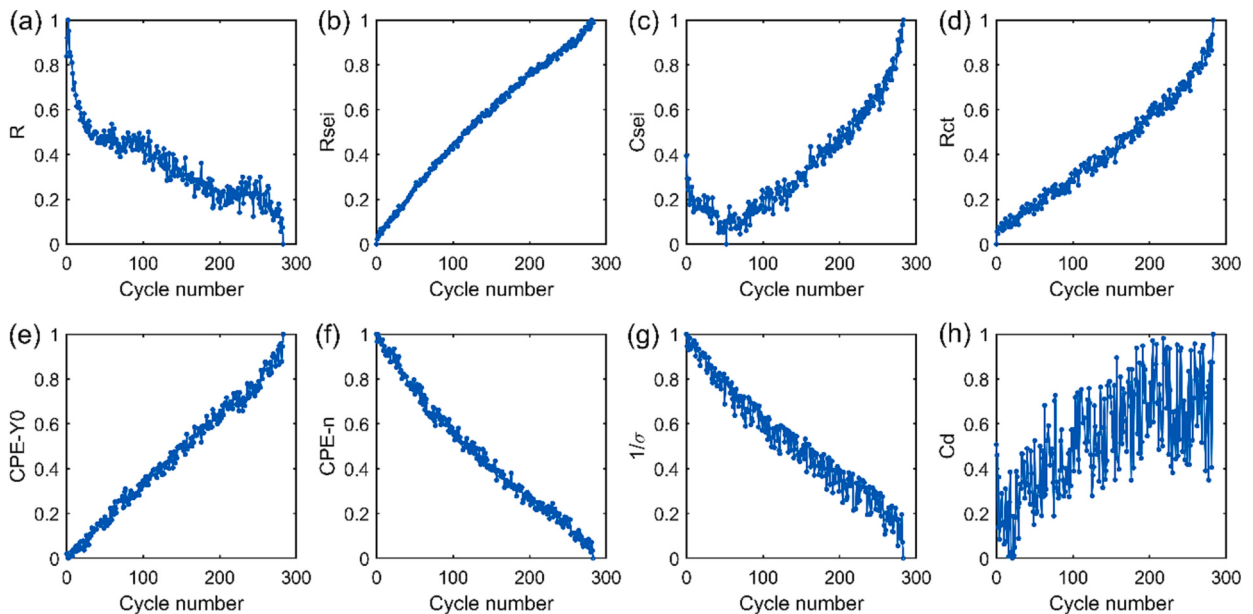
**Fig. 7.** (a) Fitting result of ECMC on the EIS data of 25C01 battery's first charge-discharge cycles. (b)-(d) Fitting results of ECMC on the EIS data of battery1–3.

$$\Delta^2 = K(x^*, X) - K(x^*, X)(K(X, X) + \sigma^2 I)^{-1} Y K(X, x^*) \quad (12)$$

which is a measure of uncertainty.

We used zero mean function and a diagonal squared exponential covariance function with ARD in GPR, the covariance function is defined as:

$$\kappa_{SE}^{ARD}(x_i, x_j) = \sigma_f^2 \exp \left[-\frac{1}{2} \sum_{m=1}^n \frac{(x_{im} - x_{jm})^T (x_{im} - x_{jm})}{\sigma_m^2} \right] \quad (13)$$

**Fig. 8.** Variation trend of proposed ECMC's normalized component parameters with battery degradation. (a) internal resistance of battery-R. (b) resistance of SEI film-R_{sei}. (c) capacitance of SEI film-C_{sei}. (d) resistance of charge transfer process-R_{ct}. (e) first parameter of CPE-Y₀. (f) second parameter of CPE-n. (g) reciprocal of Warburg coefficient-1/σ. (h) diffusion capacitor connecting in parallel with Warburg element-C_d.

where σ_m is the length scale of the input feature m , and σ_f is the signal standard deviation. By changing σ_m in the training process, different input features can obtain different weights, so as to adjust the proportion of input features' influence on the estimated result. The other hyper-parameter σ_f is also adjusted during training process.

3. SOH estimation

3.1. Variation trend of ECMC' parameters with battery degradation

In Section 1, the Nyquist plot of EIS is used to observe its change trend along with battery degradation preliminarily. However, the change trend can only be observed qualitatively according to this method, but could not be quantitatively grasped. This problem can be solved by fitting EIS data with proposed ECMC and observing the variation trend of its component parameters with battery degradation. The ECMC was used to fit more than 2000 EIS data in dataset and the fitting results showed that it could fit most of EIS data well.

After getting the fitting results, 35C01 battery was chosen to observe the influence of battery degradation on its internal structure and reaction processes. Fig. 8 shows the normalized fitting results of component parameters. For 35C01 battery, as the number of battery charge-discharge cycles increases, the corresponding 8 parameters of seven components in the ECMC change regularly. Among them, R and n show a decreasing trend with the increase of cycle number. While R_{sei} , C_{sei} , R_{ct} , Y_0 , σ , and C_d have the opposite trend. It should be noticed that the capacitor C_d , which is connected with Warburg element in parallel increases at the same time, which indicates that the degradation of battery will lead to the increase of Li-ions and electrons accumulated at the electrode. This means that the diffusion speed of Li-ions in the electrolyte is getting slower and slower, it's consistent with actual situation.

Although all of the component parameters have an obvious tendency with the increase of charge-discharge cycles, their vibration phenomenon can't be ignored either. The reason for this phenomenon may be the polarization effect of the LIBs. Although these LIBs were left to rest for 15 min after being fully charged, they had not yet reached a stable state, and the polarization effect had not been completely eliminated. As a result, the EIS data measured at this time was still not stable. In particular, the diffusion capacitor C_d has the most violent vibration phenomenon among all the parameters. This is mainly for the following

two reasons. On one hand, the impact of polarization effect on low-frequency EIS measurement is greater than that on high-frequency EIS measurement. The measurement time of low-frequency EIS measurement is much longer than that of high-frequency EIS measurement, so the polarization effect has a longer time to take effect. On the other hand, the true value of C_d is larger than that of C_{sei} and CPE, which also have the capacitive reactance effect. Values shown in Fig. 8 are normalized, but the true value of C_d is more than one order of magnitude higher than that of C_{sei} and CPE actually. Meanwhile, the larger the capacitance value, the smaller the impedance, so C_d is more susceptible to the effect of polarization effect, resulting in the emergence of variation.

3.2. Result and discussion

After the ECMC's parameters were obtained via EIS, parameters other than R were used to estimate the batteries' SOH. The reason why R was unused is because it shows a tendency to contradict the actual situation at 35 °C and 45 °C. Fig. 9 shows the variation trend of R with battery degrading for 35C01-02 and 45C01-02 batteries. As can be seen from Fig. 9, with the aging of the battery, the internal resistance R of the battery 35C01, 45C01 and 45C02 shows a decreasing trend, the 35C02 battery even shows a tendency to rise and fall at times. However, in the literature as far as we read, without exception, it is pointed out that the internal resistance R of the battery should increase as it degrades. And the appearance of this phenomenon is not caused by modeling or parameter identification, but the EIS data is inherently like this. So R was unused finally.

To verify the estimation performance of SOH by using ECMC's component parameters with GPR, the GPR was trained by constructing a training dataset $\mathcal{D} = \{(x_i, y_i), i = 1, 2, 3, \dots, n\}$ using 25C01-04, 35C01 and 45C01 batteries' data together, where $x_i = \{R_{sei}, C_{sei}, R_{ct}, Y_0, n, \sigma, C_d\}$ and y_i is the corresponding SOH. Then the 25C05-08, 35C02 and 45C02 batteries' data were used together to construct a test dataset to test it. We call this approach ECMC-GPR method. In this method, we provide GPR with specific physical meaning features associated with SOH that can be found in different temperatures and types of LIBs, which gives our approach a certain generalization ability.

To test the performance of proposed ECMC-GPR method, it was compared with the EIS-GPR method proposed in Ref [15] and the ECM

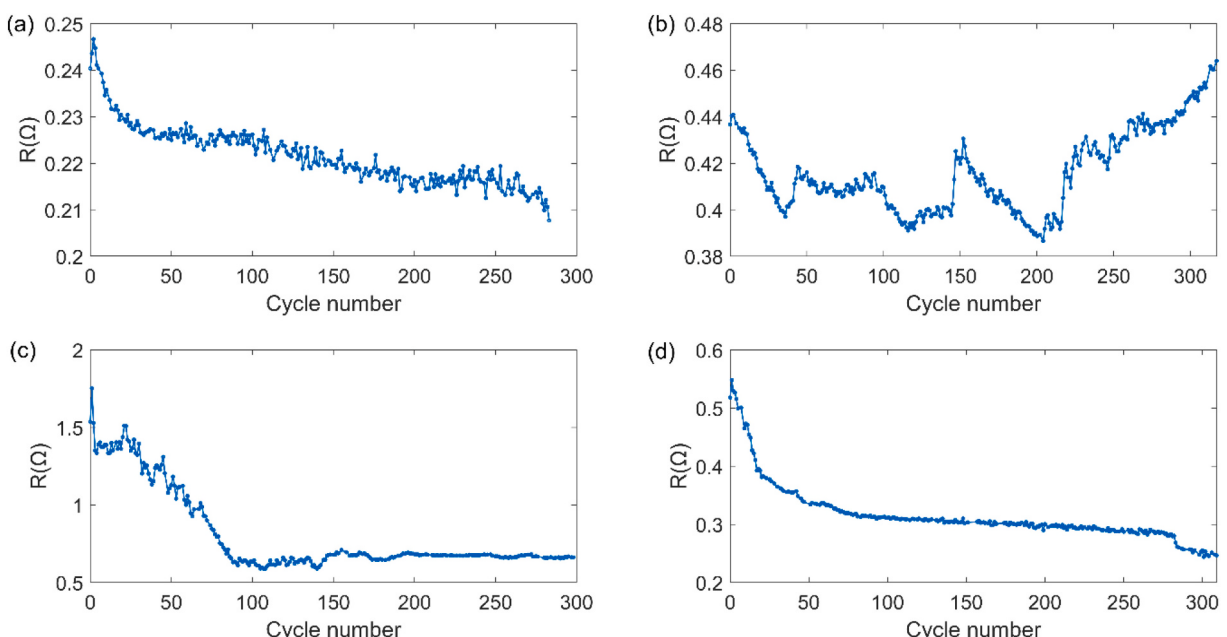


Fig. 9. (a)-(d) the variation trend of R with battery degrading for 35C01, 35C02, 45C01, 45C02 batteries.

(b)-GPR method. EIS-GPR method uses all the real and imaginary parts of EIS data as inputs to GPR directly to estimate batteries' SOH, without the feature extraction step. By comparing with this method, we can find out whether the component parameters identified by ECMC are helpful for the SOH estimation of batteries. While the ECM (b)-GPR method used the ECM (b) above-mentioned to fit EIS data, then all of the fitted parameters were employed to estimate SOH except the internal resistance R . By comparing with this method, whether the ECMC is better than other ECM can be verified, because as shown in Table 1, among the ECMs, the fitting error on EIS data for ECM (b) is the lowest. The SOH estimation results using these three methods for all six test batteries are shown in Fig. 10. A dot dash line with a slope of 1 in the middle of the figure represents the ideal case, indicating that estimated SOH for these batteries is exactly the same as actual value, and the closer a dot is to the dot dash line, the better estimation result it is. In addition, the two dotted lines on both sides of the dot dash line represent the error range of 2 % SOH. When a point lies between these two lines, it indicates that the SOH estimation error is within 2 %. As shown in Fig. 10, compared with the EIS-GPR method, the SOH estimation results of six batteries by ECMC-GPR method are closer to the dot dash line, and more points fall into the area between the dotted lines. While the performance of ECM (b)-GPR method shows the opposite trend. In other words, the SOH estimation results of the ECM (b)-GPR method are worse than those of the EIS-GPR method. That's because the poor accuracy of the features identified by ECM (b). The features identified by ECM (b) do not accurately reflect the changes in the internal structure and reaction processes of the LIB during degradation. Compared to using EIS data directly, we believe that using inaccurate features identified from EIS data will negatively affect the estimated results. On the other hand, the SOH estimation results of the ECMC-GPR method are better than the EIS-GPR method. This can be attributed to the higher correlation between the features identified from EIS data by ECMC and the SOH, compared to using EIS data at different frequencies as features directly. Higher correlated features can have a positive impact on the estimation results.

And the numerical results of above three methods for six test batteries are shown in Table 3. The comparison indexes used are mean absolute error (MAE), mean absolute percentage error (MAPE) and RMSE. For each battery, the error of the method with the smallest estimation error among these three methods will be marked in bold in the table. Compared with the other two methods, the ECMC-GPR method has better performance. Among all test batteries, the SOH estimation performance of 45C02 battery is the best, and its RMSE can reach 1.01 %. Even on the battery 25C08, which has the worst estimation performance, the ECMC-GPR method still has a significant improvement over

the other methods on all the indexes.

4. Conclusion

Accurate estimation of batteries' SOH is a very important function of BMS. At present, the mainstream method is to estimate SOH according to the charge-discharge parameters. However, these parameters such as current and voltage do not contain sufficient internal information of battery, decreasing the accuracy. Using EIS data of battery can efficiently solve this problem, but then comes the problem of how to extract effective features from EIS data. In order to solve this problem, in this paper, we speculated the internal reactions of battery under low frequency excitation, and believed that there is an EDL effect similar to SEI film inside battery in addition to Warburg impedance. Based on this, we improved the commonly used ECM and proposed the ECMC. This model can greatly improve the fitting performance of EIS data. Moreover, feature extraction of EIS data was carried out by the ECMC. Compared with other methods, the extracted features have clearer physical meaning, which can more intuitively reflect the changing trend of the batteries' internal structure and reaction processes while degrading. Finally, we used the extracted features as the inputs of GPR to estimate the SOH. Compared with the method using EIS data directly and using other ECM to fit EIS data, the accuracy of SOH estimation is greatly improved by using our ECMC-GPR method, and the RMSE could reach 1.01 % at the minimum, the average RMSE is only 1.77 %. On other indexes, ECMC-GPR method also performs better.

CRediT authorship contribution statement

Chaofan Li: Conceptualization, Methodology, Software, Validation, Investigation, Writing - original draft. **Lin Yang:** Conceptualization, Methodology, Investigation, Writing - Reviewing & Editing. **Qiang Li:** Methodology, Software, Investigation. **Qisong Zhang:** Methodology, Software, Writing - Reviewing & Editing. **Zhengyi Zhou:** Methodology, Investigation. **Yizhen Meng:** Validation, Investigation. **Xiaowei Zhao:** Methodology, Investigation, Funding acquisition. **Lin Wang:** Investigation, Funding acquisition. **Shumei Zhang:** Investigation, Funding acquisition. **Yang Li:** Investigation, Writing - Reviewing & Editing. **Feng Lv:** Investigation, Writing - Reviewing & Editing.

Declaration of competing interest

The authors declare that they have no known competing financial interests or personal relationships that could have appeared to influence

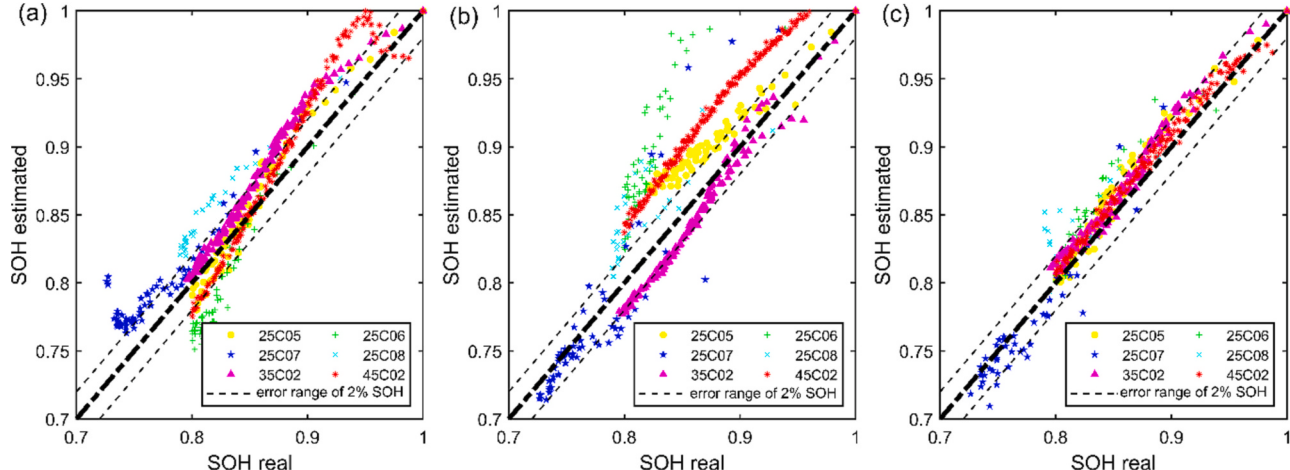


Fig. 10. (a) SOH estimation results of EIS-GPR method for all test batteries.
(b) SOH estimation results of ECM (b)-GPR method for all test batteries.
(c) SOH estimation results of ECMC-GPR method for all test batteries.

Table 3

SOH estimation errors using EIS-GPR method, ECM (b)-GPR method and ECMC-GPR method.

Cell	MAE (% SOH)			MAPE (%)			RMSE (% SOH)		
	EIS-GPR	ECM(b)-GPR	ECMC-GPR	EIS-GPR	ECM(b)-GPR	ECMC-GPR	EIS-GPR	ECM(b)-GPR	ECMC-GPR
25C05	1.19	2.99	1.23	1.39	3.49	1.43	1.54	3.19	1.48
25C06	3.16	7.25	1.69	3.88	8.73	2.01	3.50	7.91	2.14
25C07	2.65	1.94	1.27	3.48	2.41	1.62	3.04	2.83	1.73
25C08	3.50	3.45	2.35	4.30	4.26	2.90	3.61	4.03	2.95
35C02	1.87	1.58	1.16	2.16	1.87	1.35	2.13	1.7	1.31
45C02	2.11	4.70	0.92	2.34	5.37	1.05	2.63	4.73	1.01
Average	2.41	3.65	1.44	2.93	4.36	1.73	2.74	4.07	1.77

the work reported in this paper.

Data availability

We used an open dataset.

Acknowledgments

This work was supported by the Shanghai Automotive Industry Science and Technology Development Foundation (No. 2308) and National Natural Science Foundation of China (No. 51875339). The authors would like to express their appreciations for these funds.

References

- B. Scrosati, J. Garche, Lithium batteries: status, prospects and future, *J. Power Sources* 195 (9) (2010) 2419–2430, <https://doi.org/10.1016/j.jpowsour.2009.11.048>.
- H. Wu, Y. Cui, Designing nanostructured Si anodes for high energy lithium ion batteries, *Nano Today* 7 (5) (2012) 414–429, <https://doi.org/10.1016/j.nantod.2012.08.004>.
- R. Al Nazer, V. Cattin, P. Granjon, M. Montaru, M. Ranieri, Broadband identification of battery electrical impedance for hevs, *IEEE Trans Veh Technol* 62 (7) (2013) 2896–2905, <https://doi.org/10.1109/TVT.2013.2254140>.
- W. Chen, J. Liang, Z. Yang, G. Li, A review of lithium-ion battery for electric vehicle applications and beyond, *Energy Procedia* 158 (2019) 4363–4368, <https://doi.org/10.1016/j.egypro.2019.01.783>.
- Y. Song, D. Liu, H. Liao, Y. Peng, A hybrid statistical data-driven method for on-line joint state estimation of lithium-ion batteries, *Appl. Energy* 261 (2020) 114408, <https://doi.org/10.1016/j.apenergy.2019.114408>.
- S. Huang, C. Liu, H. Sun, Q. Liao, State of health estimation of lithium-ion batteries based on the regional frequency, *J. Power Sources* 518 (2022) 230773, <https://doi.org/10.1016/j.jpowsour.2021.230773>.
- P.K. Jones, U. Stimming, A.A. Lee, Impedance-based forecasting of lithium-ion battery performance amid uneven use, *Nat. Commun.* 13 (1) (2022) 4806, <https://doi.org/10.1038/s41467-022-32422-w>.
- Valentin Sulzer, Peyman Mohtat, Antti Aittio, Suhak Lee, Yen T. Yeh, Frank Steinbacher, Muhammad Umer Khan, Jang Woo Lee, Jason B. Siegel, Anna G. Stefanopoulou, David A. Howey, The challenge and opportunity of battery lifetime prediction from field data, *Joule* 5 (8) (2021) 1934–1955, <https://doi.org/10.1016/j.joule.2021.06.005>.
- G. Dong, J. Wei, A physics-based aging model for lithium-ion battery with coupled chemical/mechanical degradation mechanisms, *Electrochim. Acta* 395 (2021) 139133, <https://doi.org/10.1016/j.electacta.2021.139133>.
- F. Luo, H. Huang, L. Ni, T. Li, Rapid prediction of the state of health of retired power batteries based on electrochemical impedance spectroscopy, *J. Energy Storage* 41 (2021) 102866, <https://doi.org/10.1016/j.est.2021.102866>.
- Y. Fu, J. Xu, M. Shi, X. Mei, A fast impedance calculation-based battery state-of-health estimation method, *IEEE Trans Ind Electron* 69 (7) (2022) 7019–7028, <https://doi.org/10.1109/TIE.2021.3097668>.
- B. Bullecks, R. Suresh, R. Rengaswamy, Rapid impedance measurement using chirp signals for electrochemical system analysis, *Comput. Chem. Eng.* 106 (2017) 421–436, <https://doi.org/10.1016/j.compchemeng.2017.05.018>.
- Q. Zhang, D. Wang, B. Yang, H. Dong, C. Zhu, Z. Hao, An electrochemical impedance model of lithium-ion battery for electric vehicle application, *J. Energy Storage* 50 (2022) 104182, <https://doi.org/10.1016/j.est.2022.104182>.
- P.J. Weddle, R.J. Kee, T. Vincent, A stitching algorithm to identify wide-bandwidth electrochemical impedance spectra for li-ion batteries using binary perturbations, *J. Electrochem. Soc.* 165 (9) (2018) A1679–A1684, <https://doi.org/10.1149/2.064180jes>.
- Y. Zhang, Q. Tang, Y. Zhang, J. Wang, U. Stimming, A.A. Lee, Identifying degradation patterns of lithium ion batteries from impedance spectroscopy using machine learning, *Nat. Commun.* 11 (1) (2020) 1706, <https://doi.org/10.1038/s41467-020-15235-7>.
- T.K. Pradyumna, K. Cho, M. Kim, W. Choi, Capacity estimation of lithium-ion batteries using convolutional neural network and impedance spectra, *J. Power Electron.* 22 (5) (2022) 850–858, <https://doi.org/10.1007/s43236-022-00410-4>.
- Y. Li, B. Dong, T. Zerrin, E. Jauregui, X. Wang, X. Hu, D. Ravichandran, R. Shang, J. Xie, M. Ozkan, C. Ozkan, State-of-health prediction for lithium-ion batteries via electrochemical impedance spectroscopy and artificial neural networks, *Energy Storage* 2 (5) (2020), <https://doi.org/10.1002/est.212186>.
- T.F. Landinger, G. Schwarzerberger, A. Jossen, High frequency impedance characteristics of cylindrical lithium-ion cells: physical-based modeling of cell state and cell design dependencies, *J. Power Sources* 488 (2021) 229463, <https://doi.org/10.1016/j.jpowsour.2021.229463>.
- X. Duan, F. Liu, E. Agar, X. Jin, Parameter identification of lithium-ion batteries by coupling electrochemical impedance spectroscopy with a physics-based model, *J. Electrochem. Soc.* 169 (4) (2022) 040561, <https://doi.org/10.1149/1945-7111/ac682f>.
- Z. Wei, C. Zou, F. Leng, B.H. Soong, K.-J. Tseng, Online model identification and state-of-charge estimate for lithium-ion battery with a recursive total least squares-based observer, *IEEE Trans Ind Electron* 65 (2) (2018) 1336–1346, <https://doi.org/10.1109/TIE.2017.2736480>.
- C. Chang, S. Wang, C. Tao, J. Jiang, Y. Jiang, L. Wang, An improvement of equivalent circuit model for state of health estimation of lithium-ion batteries based on mid-frequency and low-frequency electrochemical impedance spectroscopy, *Measurement* 202 (2022) 111795, <https://doi.org/10.1016/j.measurement.2022.111795>.
- M. Galeotti, L. Cinà, C. Giannamico, S. Cordiner, A. Di Carlo, Performance analysis and soh (state of health) evaluation of lithium polymer batteries through electrochemical impedance spectroscopy, *Energy* 89 (2015) 678–686, <https://doi.org/10.1016/j.energy.2015.05.148>.
- D. Li, D. Yang, L. Li, L. Wang, K. Wang, Electrochemical impedance spectroscopy based on the state of health estimation for lithium-ion batteries, *Energies* 15 (18) (2022) 6665, <https://doi.org/10.3390/en15186665>.
- Q. Zhang, L. Yang, W. Guo, J. Qiang, C. Peng, Q. Li, Z. Deng, A deep learning method for lithium-ion battery remaining useful life prediction based on sparse segment data via cloud computing system, *Energy* 241 (2022) 122716, <https://doi.org/10.1016/j.energy.2021.122716>.
- Z. Lyu, R. Gao, A model-based and data-driven joint method for state-of-health estimation of lithium-ion battery in electric vehicles, *Int. J. Energy Res.* (2019) er.4784, <https://doi.org/10.1002/er.4784>.
- K. Ouyang, Y. Fan, M. Yazdi, W. Peng, Data-driven-based internal temperature estimation for lithium-ion battery under variant state-of-charge via electrochemical impedance spectroscopy, *Energ. Technol.* 10 (3) (2022) 2100910, <https://doi.org/10.1002/ente.202100910>.
- J. Obregon, Y.-R. Han, C.W. Ho, D. Mouraliraman, C.W. Lee, J.-Y. Jung, Convolutional autoencoder-based soh estimation of lithium-ion batteries using electrochemical impedance spectroscopy, *J. Energy Storage* 60 (2023) 106680, <https://doi.org/10.1109/j.est.2023.106680>.
- B. Jiang, J. Zhu, X. Wang, X. Wei, W. Shang, A comparative study of different features extracted from electrochemical impedance spectroscopy in state of health estimation for lithium-ion batteries, *Appl. Energy* 322 (2022) 119502, <https://doi.org/10.1016/j.apenergy.2022.119502>.
- C. Chang, C. Wang, S. Jiang, J. Yao, G. Y, Jiang Y, Liao L, Lithium-ion battery state of health estimation based on electrochemical impedance spectroscopy and cuckoo search algorithm optimized elman neural network, *J. Electrochem. Energy Convers. Storage* [no date]: 11.
- Y. Zhou, G. Dong, Q. Tan, X. Han, C. Chen, J. Wei, State of health estimation for lithium-ion batteries using geometric impedance spectrum features and recurrent gaussian process regression, *Energy* 262 (2023) 125514, <https://doi.org/10.1016/j.energy.2022.125514>.
- X. Su, B. Sun, J. Wang, W. Zhang, S. Ma, X. He, H. Ruan, Fast capacity estimation for lithium-ion battery based on online identification of low-frequency electrochemical impedance spectroscopy and gaussian process regression, *Appl. Energy* 322 (2022) 119516, <https://doi.org/10.1016/j.apenergy.2022.119516>.
- C. Zhang, Y. Zhu, G. Dong, J. Wei, Data-driven lithium-ion battery states estimation using neural networks and particle filtering, *Int. J. Energy Res.* (2019) er.4820, <https://doi.org/10.1002/er.4820>.
- M. Adaikappan, N. Sathiayamoorthy, Modeling, state of charge estimation, and charging of lithium-ion battery in electric vehicle: a review, *Int. J. Energy Res.* 46 (3) (2022) 2141–2165, <https://doi.org/10.1002/er.7339>.
- D.N.T. How, M.A. Hannan, M.S. Hossain Lipu, P.J. Ker, State of charge estimation for lithium-ion batteries using model-based and data-driven methods: a review,

- IEEE Access 7 (2019) 136116–136136, <https://doi.org/10.1109/ACCESS.2019.2942213>.
- [35] L. Cai, J. Meng, D.-I. Stroe, J. Peng, G. Luo, R. Teodorescu, Multiobjective optimization of data-driven model for lithium-ion battery soh estimation with short-term feature, IEEE Trans. Power Electron. 35 (11) (2020) 11855–11864, <https://doi.org/10.1109/TPEL.2020.2987383>.
- [36] X. Pang, R. Huang, J. Wen, Y. Shi, J. Jia, J. Zeng, A lithium-ion battery rul prediction method considering the capacity regeneration phenomenon, Energies 12 (12) (2019) 2247, <https://doi.org/10.3390/en12122247>.
- [37] R.B. Wright, J.P. Christophersen, C.G. Motloch, J.R. Belt, C.D. Ho, V.S. Battaglia, J. A. Barnes, T.Q. Duong, R.A. Sutula, Power fade and capacity fade resulting from cycle-life testing of advanced technology development program lithium-ion batteries, J. Power Sources 119–121 (2003) 865–869, [https://doi.org/10.1016/S0378-7753\(03\)00190-3](https://doi.org/10.1016/S0378-7753(03)00190-3).
- [38] C. Huang, X. Zhao, S. Liu, Y. Hao, Q. Tang, A. Hu, Z. Liu, X. Chen, Stabilizing zinc anodes by regulating the electrical double layer with saccharin anions, Adv. Mater. 33 (38) (2021) 2100445, <https://doi.org/10.1002/adma.202100445>.
- [39] R.R. Richardson, C.R. Birk, M.A. Osborne, D.A. Howey, Gaussian process regression for in situ capacity estimation of lithium-ion batteries, IEEE Trans. Industr. Inform. 15 (1) (2019) 127–138, <https://doi.org/10.1109/TII.2018.2794997>.